ChemComm

Accepted Manuscript

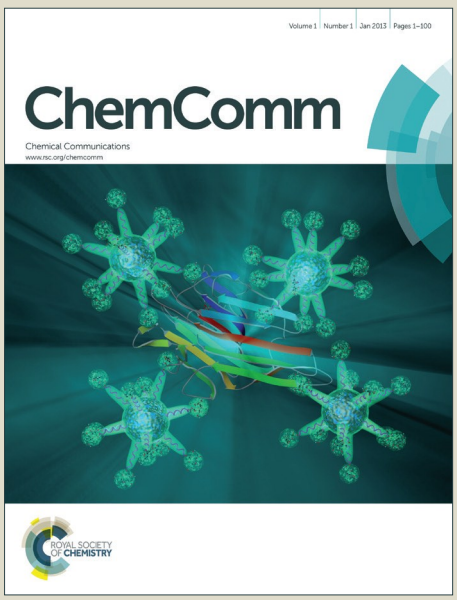

ROYAL SOCIETY OF CHEMISTRY

www.rsc.org/chemcomm

Journal Name

COMMUNICATION

Creating a synergistic interplay between tubular MoS_2 and particulate Fe_3O_4 for improved lithium storage†

Received 00th January 20xx,
Accepted 00th January 20xx

DOI: 10.1039/x0xx00000x

www.rsc.org/

Xiao-Dong Zhu,[a] Ke-Xin Wang,[b] Du-Juan Yan,[b] Shi-Ru Le,[a] Ru-Jia Ma,[b] Ke-Ning Sun*[a] and Yi-Tao Liu*[c]

A novel three-dimensional MoS_2@Fe_3O_4 nanohybrid, composed of tubular MoS_2 uniformly and densely decorated with particulate Fe_3O_4, is constructed which exhibits significantly improved lithium storage performances through an impressive synergistic interplay between the two active materials.

Inorganic graphene analogues (IGAs) such as transition metal dichalcogenides (*e.g.*, MoS_2 and WS_2)[1,2] and oxides (*e.g.*, MnO_2)[3] are emerging as fascinating anode candidates for next-generation, high-power lithium-ion batteries (LIBs) due to their rich resources, low toxicity and extraordinarily high theoretical capacities arising from a unique "conversion reaction" mechanism. In this mechanism, 4–8 Li^+ ions can be stored per formula unit since the oxidation state of a high-valance transition metal compound is fully utilised. It is worth noting, however, that these layered materials are all featured by large surface areas and high surface energies, which translate into strong interlayer van der Waals forces giving rise to a huge tendency to restack. If so, large quantities of active sites for lithium storage are sacrificed, and poor cycle and rate performances are inevitable. Therefore, various hollow micro/nanostructures of IGAs are being pursued for improved electrochemical performances.[4]

MoS_2, as a typical member of transition metal dichalcogenides, is composed of a layer of molybdenum atoms sandwiched between two layers of sulphur atoms, which are covalently bonded to form a nanosheet. The reasonably high theoretical capacity (670 mA h g^{-1}) of MoS_2, resulting from a conversion reaction of $MoS_2 + 4Li^+ + 4e^- \rightarrow Mo + 2Li_2S$, may rank it as a promising substitute for graphitic carbon — the current anode material of LIBs that has a relatively low theoretical capacity (372 mA h g^{-1}). Unfortunately, the MoS_2 nanosheets suffer from huge volume expansion as well as serious restacking during repeated lithiation/delithiation, which are major reasons for the poor cyclability especially at high rates. One possible solution is to employ different spacers such as graphene nanosheets,[5] carbon nanotubes,[6] carbon nanospheres,[7] noble metal nanoparticles,[8] and transition metal oxide nanoparticles,[9] which can physically isolate the MoS_2 nanosheets for reversible lithium and electron transport. Another strategy is to construct higher-level hollow assemblies from the MoS_2 nanosheets, *e.g.*, nanotubes,[10] nanoboxes,[11] and hollow nanospheres,[12] which are expected to improve the reversible capacity of MoS_2 by alleviating the restacking of the nanosheets. For example, in a recent report, Wang *et al.* have fabricated interesting tubular architectures from the MoS_2 nanosheets, which deliver a ~40% higher reversible capacity after 50 charging–discharging cycles at a current density of 100 mA g^{-1}.[10] However, it should be stressed that the cycle stability of tubular MoS_2 is still not satisfactory due to a certain degree of aggregation, exhibiting an obvious and steady capacity decay from the very beginning. In this regard, further improvement is necessary to achieve better cycle and rate performances.

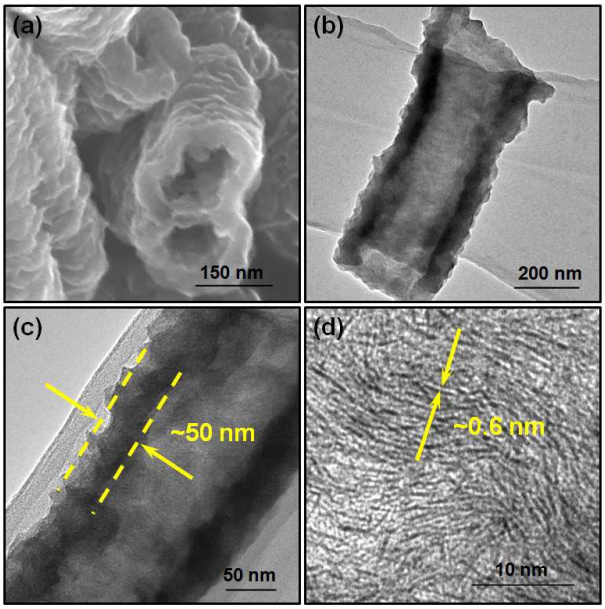

Fig. 1 – (a) SEM, (b and c) TEM, and (d) HRTEM images of as-synthesised tubular MoS_2.

[a] *Academy of Fundamental and Interdisciplinary Sciences, Harbin Institute of Technology, Harbin 150080, China. E-mail: keningsunhit@126.com*
[b] *Department of Chemistry, Harbin Institute of Technology, Harbin 150001, China.*
[c] *Key Laboratory of Advanced Materials (MOE), Department of Chemical Engineering, Tsinghua University, Beijing 100084, China. E-mail: liu-yt03@mails.tsinghua.edu.cn*

† Electronic Supplementary Information (ESI) available: [Experimental details and supplementary figures]. See DOI: 10.1039/x0xx00000x

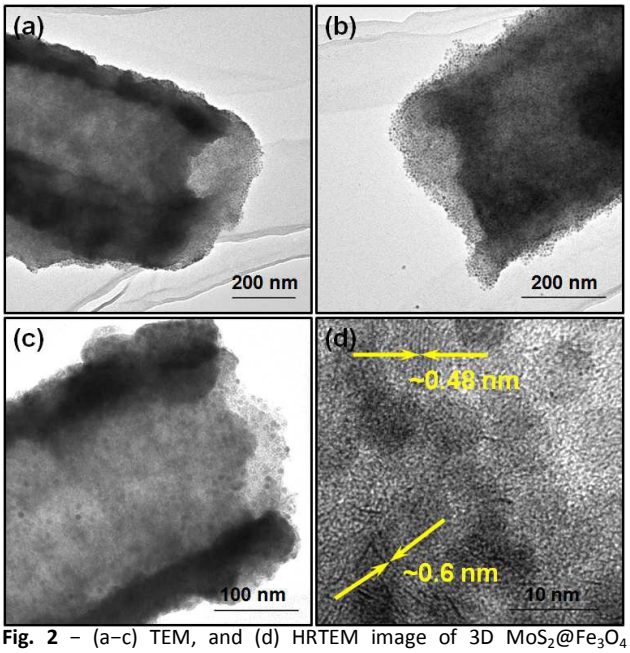

Fig. 2 – (a–c) TEM, and (d) HRTEM image of 3D MoS_2@Fe_3O_4 nanohybrid at an Fe_3O_4/MoS_2 wt ratio of 1/2.

Here we report a novel hybridisation design, by which a second active material, *i.e.*, particulate Fe_3O_4 is hierarchically assembled on tubular MoS_2 by a facile, one-step approach based on van der Waals interactions.[13] The resulting three-dimensional (3D) MoS_2@Fe_3O_4 nanohybrid, composed of tubular MoS_2 uniformly and densely decorated with particulate Fe_3O_4, exhibits significantly improved reversible capacity and rate capabilities through a synergistic interplay between the two active materials. On one hand, tubular MoS_2 serving as a matrix can provide abundant mesopores and hollow interiors to facilitate lithium transport and storage, and buffer the structural stress during the cycling processes. On the other hand, particulate Fe_3O_4 acting as a spacer can isolate tubular MoS_2 from aggregation, thereby increasing the intertube distance for easy lithium access. Moreover, compared to other spacers such as nanocarbons and noble metals, Fe_3O_4 is particularly attractive due to its high theoretical capacity (928 mA h g^{-1}),[14] making it an important electrochemical contributor. A strikingly high reversible capacity of 1113 mA h g^{-1}@100 mA g^{-1} is delivered after 100 charging–discharging cycles, ~44% higher than that of tubular MoS_2. This value warrants our 3D MoS_2@Fe_3O_4 nanohybrid an appealing choice for high-performance LIB anode.

Tubular MoS_2 is synthesised by a hydrothermal method,[10] and its morphological information is provided in **Fig. 1a** and **S1** (ESI†). From these SEM images we can clearly see uniform tubular architectures with ripple-like surfaces and hollow interiors, whose outer diameters are ~200 nm and lengths are above 1 μm. The same morphology is confirmed by TEM characterisation, as shown in **Fig. 1b**. Under closer examination (**Fig. 1c**), a wall thickness of ~50 nm can be recognised. Ambiguously, the tubular architectures are constructed from numerous MoS_2 nanosheets, most of which are indeed single layers since the observed wrinkles marking these MoS_2 nanosheets are randomly distributed without obvious "stacking" traces (**Fig. 1d**). Moreover, the measured interlayer distance of ~0.6 nm further proves the presence of single-layer MoS_2 nanosheets. The XRD result of tubular MoS_2, as presented in **Fig. S2** (ESI†), is in good agreement with TEM characterisation. The diffraction peaks located at 2θ = 33° and 59° are assigned to the (100) and (110) planes of 2H–MoS_2 polytype, respectively. The absence of (002) diffraction peak, different from that of bulk MoS_2, indicates that the well-stacked layers have been successfully exfoliated.[10]

Particulate Fe_3O_4 with an average diameter of ~6 nm is synthesised according to our previous report.[13] For the hierarchical assembly, the two building blocks are mixed in tetrahydrofuran (THF) under sonication, during which particulate Fe_3O_4 is spontaneously attracted to the naked surfaces of tubular MoS_2 by strong van der Waals forces. As explored by us previously, the solvent property plays a key role in determining the assembly result: since THF is a bad solvent for MoS_2, the high surface energy of this layered material cannot be compensated for in an unsolvated state, and a huge tendency to aggregate exists.[13] Once organically modified particulate Fe_3O_4 featured by a low surface energy is introduced, it is spontaneously attracted to the naked surfaces of tubular MoS_2 by strong van der Waals forces, thereby serving as a spacer to isolate the latter from aggregation as well as reducing the total free energy. It should be stressed that this assembly approach based on van der Waals interactions is facile and cost-effective compared to those based on hydrothermal reactions[9a,15] and complexation interactions.[16] **Fig. 2** shows TEM and HRTEM images of the resulting 3D MoS_2@Fe_3O_4 nanohybrid at an Fe_3O_4/MoS_2 wt ratio of 1/2. As seen from the TEM images, tubular MoS_2 is uniformly and densely decorated with particulate Fe_3O_4. Note that the hierarchical assembly is highly efficient since no free nanoparticles are seen dissociated from tubular MoS_2. **Fig. 2d** presents an HRTEM image of the 3D MoS_2@Fe_3O_4 nanohybrid. The coexistence of the two building blocks can be easily identified, with measured lattice fringe distances of ~0.48 and ~0.6 nm corresponding to the (111) and (002) planes of spinel Fe_3O_4 and 2H–MoS_2, respectively. This novel hybridisation design can fully exploit the merits of the two building blocks through a synergistic interplay: 1) tubular MoS_2 serves as a matrix to provide abundant mesopores and hollow interiors, thus facilitating lithium transport and storage; 2) particulate Fe_3O_4 acts as a spacer to effectively isolate tubular MoS_2 from aggregation, thereby increasing the intertube distance for easy lithium access. Moreover, the extremely high theoretical capacities of the two building blocks rank them as excellent active materials whose combination may lead to optimised lithium storage performances. For comparison, the Fe_3O_4/MoS_2 wt ratio is further elevated to 1/1, and typical TEM images are presented in **Fig. S4** (ESI†). It can be seen that the distribution of particulate Fe_3O_4 on tubular MoS_2 is much denser than the case shown in **Fig. 2**. Besides, large quantities of free nanoparticles unbound to the naked surfaces of tubular MoS_2 can be observed, which demonstrates that particulate Fe_3O_4 is excess relative to tubular MoS_2, and an "over-saturated" situation is therefore reached at this wt ratio. As such, we conclude that an Fe_3O_4/MoS_2 wt ratio of 1/2 is the optimum value for uniform and complete coverage without "over-dosing".

To further explore the interactions between tubular MoS_2 and particulate Fe_3O_4 in the 3D MoS_2@Fe_3O_4 nanohybrid, we present high-resolution Mo 3d, S 2p, Fe 2p and O 1s XPS spectra in **Fig. 3**. It can be seen that for tubular MoS_2, the Mo 3d spectrum has

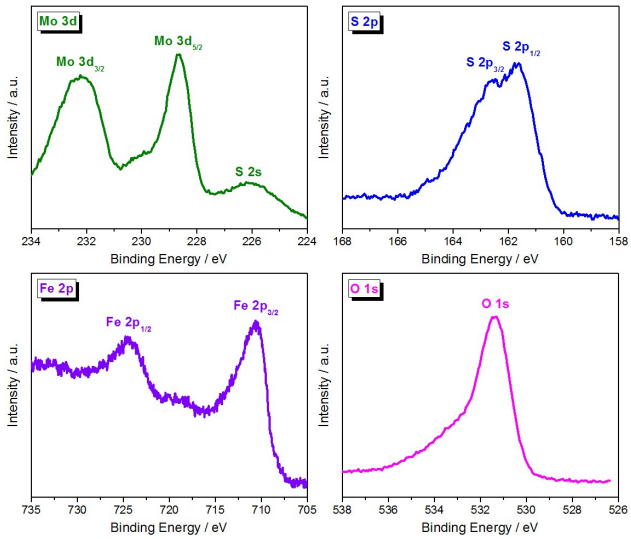

Fig. 3 – High-resolution Mo 3d, S 2p, Fe 2p and O 1s XPS spectra of 3D MoS_2@Fe_3O_4 nanohybrid at an Fe_3O_4/MoS_2 wt ratio of 1/2.

two major peaks at 232.2 and 228.7 eV, which are attributed to the doublet Mo $3d_{3/2}$ and $3d_{5/2}$ orbitals; the peaks corresponding to the S $2p_{1/2}$ and $2p_{3/2}$ orbitals of divalent sulphide ions (S^{2-}) are observed at 162.6 and 161.7 eV.[10] The binding energy profiles and positions of Mo and S in tubular MoS_2 are very similar to what are reported for neat MoS_2 nanosheets.[17] As to particulate Fe_3O_4, the two distinct peaks at 724.5 and 710.5 eV corresponding to the Fe $2p_{1/2}$ and $2p_{3/2}$ orbitals, and the peak at 530.5 eV corresponding to the O 1s orbital are also similar to the XPS spectra of neat Fe_3O_4 nanoparticles.[14b,k] There is no satellite peak located at ~719 eV, thus ruling out the presence of maghemite (Fe_2O_3).[18] The XPS results demonstrate that our facile, one-step assembly approach based on van der Waals interactions is non-invasive without altering the chemical nature of the two building blocks.

The electrochemical characteristics of the 3D MoS_2@Fe_3O_4 nanohybrid can be figured out by analysing its CV curves, as shown in **Fig. 4a**. The reduction peaks at 1.28 and 0.76 V in the 1st cathodic scan originate from the formation of $Li_xFe_3O_4$ and Li_xMoS_2 due to Li^+ intercalation. The reduction peak at 0.40 V corresponds to the conversion of Fe_3O_4 to Fe. The strong reduction peak at 0.28 V is related to the kinetically activated electrolyte degradation as well as the conversion of MoS_2 to Mo (accompanied by the formation of a Li_2S matrix). In the subsequent cathodic scan, the obvious peak at 0.28 V is negatively shifted to 0.12 V and becomes very small, indicating that the solid–electrolyte interface (SEI) film has been built perfectly. The reduction peak at 0.40 V is positively shifted to 0.69 V due to the structural modification after the 1st cycle.[19] The weak reduction peak at 0.76 V even disappears. Note that during the 2nd cathodic scan, a new reduction peak at 1.44 V arises, which is related to the conversion of S to Li_2S. In summary, the reduction peaks at 0.12, 0.69 and 1.44 V can be ascribed to the following three conversion reactions: $MoS_2 + 4Li^+ + 4e^- \rightarrow Mo + 2Li_2S$, $Fe_3O_4 + 8Li^+ + 8e^- \rightarrow 3Fe + 4Li_2O$ and $4Li^+ + 2S + 4e^- + Mo \rightarrow 2Li_2S + Mo$. In the anodic scans, the reversible oxidation peak at 2.41 V corresponds to the conversion of Li_2S to S.[8a] The broad oxidation peak at 1.54−1.90 V is the overlapping of two peaks that stand for the partial oxidation of Mo to MoS_2 and the oxidation of Fe to Fe_3O_4, respectively. Since the polarisation (1.52 V) between reduction and oxidation of the Mo^{4+}/Mo redox couple is much higher than that (0.97 V) of S/S^{2-}, the conversion between Li_2S and S should be the major reaction mode here.[20] Therefore, the major reaction mechanisms of the 3D MoS_2@Fe_3O_4 nanohybrid are the conversion reactions of $4Li^+ + 2S + 4e^- + Mo \leftrightarrow 2Li_2S + Mo$ and $Fe_3O_4 + 8Li^+ + 8e^- \leftrightarrow 3Fe + 4Li_2O$. These results are in good agreement with the corresponding charging–discharging curves (**Fig. 4b**).

To confirm the superiority of the 3D MoS_2@Fe_3O_4 nanohybrid over tubular MoS_2 in the lithium storage performances, we compare their cycle behaviours in **Fig. 4c**. Clearly, tubular MoS_2 delivers an initial capacity of 1369 mA h g^{-1}, even higher than its theoretical value due to abundant mesopores as well as defect sites (arising from low crystallinity) for lithium storage. However, an obvious capacity decay is witnessed, and the capacity drops to 772 mA h g^{-1} after 100 charging–discharging cycles, accounting for a cycle retention of only 56%. This phenomenon is in consistent with the previous report,[10] and is probably due to a certain degree of aggregation originating from strong intertube van der Waals forces. After aggregation, a substantial fraction of active sites are no longer available. To address this inherent deficiency, particulate Fe_3O_4 is hierarchically assembled on tubular MoS_2, thus forming the 3D MoS_2@Fe_3O_4 nanohybrid to achieve a synergistic interplay between the two active materials. By this novel hybridisation design, tubular MoS_2 serving as a matrix can provide abundant mesopores and hollow interiors to facilitate lithium transport and storage. The introduction of particulate Fe_3O_4 as a spacer can isolate tubular MoS_2 from aggregation, thereby increasing the intertube distance for easy lithium access. Moreover, we stress that compared to other spacers, Fe_3O_4 is particularly attractive due to its excellent electrochemical activities.[14] In consequence, the 3D MoS_2 @Fe_3O_4 nanohybrid possesses enhanced cyclability, delivering a reversible capacity up to 1113 mA h g^{-1} at the end of 100 charging–discharging cycles which accounts for a cycle retention up to 71%. This value is ~44% higher than the reversible capacity of tubular MoS_2.

Furthermore, the 3D MoS_2@Fe_3O_4 nanohybrid also exhibits significantly improved rate capabilities, delivering fairly high reversible capacities of 1183, 1110, 1019 and 910 mA h g^{-1} when cycled at current densities of 100, 200, 500 and 1000 mA g^{-1}. When the current density is raised to 2000 mA g^{-1}, the reversible capacity is still as high as 800 mA h g^{-1}. It is worth mentioning that even after deep cycling at 2000 mA g^{-1}, the reversible capacity can return to 1101 mA h g^{-1} immediately when the current density is recovered to 100 mA g^{-1}, further confirming enhanced cyclability due to the unique structural arrangement between tubular MoS_2 and particulate Fe_3O_4. In contrast, when tubular MoS_2 alone is tested under the same current densities, it delivers reversible capacities of 1070, 944, 824, 641 and 484 mA h g^{-1}, significantly lower than those of the 3D MoS_2@Fe_3O_4 nanohybrid. The superior cycle and rate performances of the 3D MoS_2@Fe_3O_4 nanohybrid therefore justify an impressive synergistic interplay between tubular MoS_2 and particulate Fe_3O_4. In this sense, our hybridisation design lays a basis for elaborate combination of different active materials into multifunctional nanohybrids with significantly improved lithium storage performances over single-component anode systems.

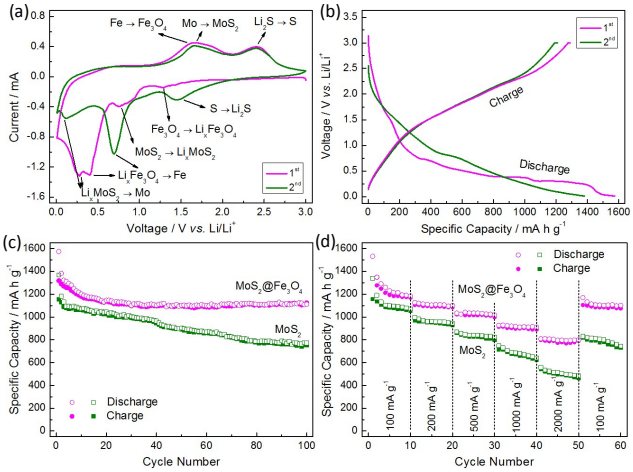

Fig. 4 – (a) CV and (b) charging–discharging curves of 3D MoS_2@Fe_3O_4 nanohybrid, (c) cycle behaviours (current density = 100 mA g^{-1}) of 3D MoS_2@Fe_3O_4 nanohybrid and tubular MoS_2, and (d) rate capabilities of 3D MoS_2@Fe_3O_4 nanohybrid.

In conclusion, an impressive synergistic interplay between tubular MoS_2 and particulate Fe_3O_4 is created, resulting in a novel 3D MoS_2@Fe_3O_4 nanohybrid. On one hand, tubular MoS_2 serving as a matrix can provide abundant mesopores and hollow interiors to facilitate lithium transport and storage and buffer the structural stress during the cycling processes. On the other hand, particulate Fe_3O_4 acting as a spacer can isolate tubular MoS_2 from aggregation, thereby increasing the intertube distance for easy lithium access. The 3D MoS_2@Fe_3O_4 nanohybrid delivers a reversible capacity as high as 1113 mA h g^{-1}@100 mA g^{-1}, ~44% higher than that of tubular MoS_2. This interesting hybridisation design may open the door to a new class of multifunctional nanohybrids as appealing choices of high-performance LIB anodes.

We thank NSFC (21304053) for financial support. X.-D.Z. is grateful to the Natural Science Foundation of Heilongjiang (B2012 02), the Fundamental Research Funds for the Central Universities (HIT.NSRIF.2013.059) and the Postdoctoral Science–Research Development Foundation of Heilongjiang (LBH-Q11130).

Notes and references

1 a) G. Du, Z. Guo, S. Wang, R. Zeng, Z. Chen and H. Liu, *Chem. Commun.*, 2010, **46**, 1106; b) H. Li, W. Li, L. Ma, W. Chen and J. Wang, *J. Alloy. Compd.*, 2009, **471**, 442.

2 a) D. Chen, G. Ji, B. Ding, Y. Ma, B. Qu, W. Chen and J. Y. Lee, *Nanoscale*, 2013, **5**, 7890; b) K. Shiva, H. S. S. Ramakrishna Matte, H. B. Rajendra, A. J. Bhattacharyya and C. N. R. Rao, *Nano Energy*, 2013, **2**, 787; c) Y. Liu, W. Wang, Y. Wang and X. Peng, *Nano Energy*, 2014, **7**, 25; d) H. Liu, D. Su, G. Wang and S. Z. Qiao, *J. Mater. Chem.*, 2012, **22**, 17437; e) X. Fang, C. Hua, C. Wu, X. Wang, L. Shen, Q. Kong, J. Wang, Y. Hu, Z. Wang and L. Chen, *Chem.–Eur. J.*, 2013, **19**, 5694.

3 a) M. Kundu, C. C. A. Ng, D. Y. Petrovykh and L. Liu, *Chem. Commun.*, 2013, **49**, 8459; b) L. Li, A.-R. O. Raji and J. M. Tour, *Adv. Mater.*, 2013, **25**, 6298; c) J. Zhu, J. Jiang, W. Ai, Z. Fan, X. Huang, H. Zhang and T. Yu, *Nanoscale*, 2014, **6**, 12990; d) T. Yang, T. Qian, M. Wang, J. Liu, J. Zhou, Z. Sun, M. Chen and C. Yan, *J. Mater. Chem. A*, 2015, **3**, 6291; e) C. X. Guo, M. Wang, T. Chen, X. W. Lou and C. M. Li, *Adv. Energy Mater.*, 2011, **1**, 736; f) L. Pan, K.-X. Wang, X.-D. Zhu, X.-M. Xie and Y.-T. Liu, *J. Mater. Chem. A*, 2015, **3**, 6477.

4 a) Z. Wang, L. Zhou and X. W. Lou, *Adv. Mater.*, 2012, **24**, 1903; b) H. B. Wu, J. S. Chen, H. H. Hng and X. W. Lou, *Nanoscale*, 2012, **4**, 2526; c) M.-R. Gao, Y.-F. Xu, J. Jiang and S.-H. Yu, *Chem. Soc. Rev.*, 2013, **42**, 2986.

5 a) Y.-T. Liu, X.-D. Zhu, Z.-Q. Duan and X.-M. Xie, *Chem. Commun.*, 2013, **49**, 10305; b) X. Zhou, L.-J. Wan and Y.-G. Guo, *Chem. Commun.*, 2013, **49**, 1838; c) K. Chang and W. Chen, *Chem. Commun.*, 2011, **47**, 4252; d) J. Ye, L. Ma, W. Chen, Y. Ma, F. Huang, C. Gao and J. Y. Lee, *J. Mater. Chem. A*, 2015, **3**, 6884; e) Z. Wang, T. Chen, W. Chen, K. Chang, L. Ma, G. Huang, D. Chen and J. Y. Lee, *J. Mater. Chem. A*, 2013, **1**, 2202; f) G. Huang, T. Chen, W. Chen, Z. Wang, K. Chang, L. Ma, F. Huang, D. Chen and J. Y. Lee, *Small*, 2013, **9**, 3693; g) Z.-Q. Duan, Y.-C. Sun, Y.-T. Liu, X.-M. Xie and X.-D. Zhu, *RSC Adv.*, 2014, **4**, 41543; h) D. Kong, H. He, Q. Song, B. Wang, W. Lv, Q.-H. Yang and L. Zhi, *Energy Environ. Sci.*, 2014, **7**, 3320.

6 a) C. Lu, W. Liu, H. Li and B. K. Tay, *Chem. Commun.*, 2014, **50**, 3338; b) K. Bindumadhavan, S. K. Srivastava and S. Mahanty, *Chem. Commun.*, 2013, **49**, 1823; c) J.-Z. Wang, L. Lu, M. Lotya, J. N. Coleman, S.-L. Chou, H.-K. Liu, A. I. Minett and J. Chen, *Adv. Energy Mater.*, 2013, **3**, 798; d) S.-K. Park, S.-H. Yu, S. Woo, B. Quan, D.-C. Lee, M. K. Kim, Y.-E. Sung and Y. Piao, *Dalton Trans.*, 2013, **42**, 2399; e) C. Zhu, X. Mu, P. A. van Aken, J. Maier and Y. Yu, *Adv. Energy Mater.*, 2015, **5**, 1401170; f) S. Ding, J. S. Chen and X. W. Lou, *Chem.–Eur. J.*, 2011, **17**, 13142.

7 L. Zhang and X. W. Lou, *Chem.–Eur. J.*, 2014, **20**, 5219.

8 L. Pan, Y.-T. Liu, X.-M. Xie and X.-D. Zhu, *Chem.–Asian J.*, 2014, **9**, 1519.

9 a) Y. Chen, B. Song, X. Tang, L. Lu and J. Xue, *Small*, 2014, **10**, 1536; b) B. Guo, K. Yu, H. Fu, Q. Hua, R. Qi, H. Li, H. Song, S. Guo and Z. Zhu, *J. Mater. Chem. A*, 2015, **3**, 6392; c) X. Li, W. Li, M. Li, P. Cui, D. Chen, T. Gengenbach, L. Chu, H. Liu and G. Song, *J. Mater. Chem. A*, 2015, **3**, 2762; d) X. Xu, Z. Fan, S. Ding, D. Yu and Y. Du, *Nanoscale*, 2014, **6**, 5245.

10 P. Wang, H. Sun, Y. Ji, W. Li and X. Wang, *Adv. Mater.*, 2014, **26**, 964.

11 L. Zhang, H. B. Wu, Y. Yan, X. Wang and X. W. Lou, *Energy Environ. Sci.*, 2014, **7**, 3302.

12 S. Ding, D. Zhang, J. S. Chen and X. W. Lou, *Nanoscale*, 2012, **4**, 95.

13 a) L. Pan, X.-D. Zhu, X.-M. Xie and Y.-T. Liu, *Adv. Funct. Mater.*, 2015, **25**, 3341; b) L. Pan, X.-D. Zhu, X.-M. Xie and Y.-T. Liu, *J. Mater. Chem. A*, 2015, **3**, 2726.

14 a) B. Wang, H. B. Wu, L. Zhang and X. W. Lou, *Angew. Chem. Int. Ed.*, 2013, **52**, 4165; b) W. Wei, S. Yang, H. Zhou, I. Lieberwirth, X. Feng and K. Müllen, *Adv. Mater.*, 2013, **25**, 2909; c) J. Luo, J. Liu, Z. Zeng, C. F. Ng, L. Ma, H. Zhang, J. Lin, Z. Shen and H. J. Fan, *Nano Lett.*, 2013, **13**, 6136; d) S. Wu, Z. Wang, C. He, N. Zhao, C. Shi, E. Liu and J. Li, *J. Mater. Chem. A*, 2013, **1**, 11011; e) Y. Su, S. Li, D. Wu, F. Zhang, H. Liang, P. Gao, C. Cheng and X. Feng, *ACS Nano*, 2012, **6**, 8349; f) S. Saadat, J. Zhu, D. H. Sim, H. H. Hng, R. Yazami and Q. Yan, *J. Mater. Chem. A*, 2013, **1**, 8672; g) S. Zhang, W. Li, B. Tan, S. Chou, Z. Li and S. Dou, *J. Mater. Chem. A*, 2015, **3**, 4793; h) D. Chen, G. Ji, Y. Ma, J. Y. Lee and J. Lu, *ACS Appl. Mater. Interfaces*, 2011, **3**, 3078; i) Z. Zhang, F. Wang, Q. An, W. Li and P. Wu, *J. Mater. Chem. A*, 2015, **3**, 7036; j) Y. Chen, H. Xia, L. Lu and J. Xue, *J. Mater. Chem.*, 2012, **22**, 5006.

15 Z. Cheng, B. He and L. Zhou, *J. Mater. Chem. A*, 2015, **3**, 1042.

16 Y.-T. Liu, Z.-Q. Duan, X.-M. Xie and X.-Y. Ye, *Chem. Commun.*, 2013, **49**, 1642.

17 K.-K. Liu, W. Zhang, Y.-H. Lee, Y.-C. Lin, M.-T. Chang, C.-Y. Su, C.-S. Chang, H. Li, Y. Shi, H. Zhang, C.-S. Lai and L.-J. Li, *Nano Lett.*, 2012, **12**, 1538.

18 J. Luo, X. Xia, Y. Luo, C. Guan, J. Liu, X. Qi, C. F. Ng, T. Yu, H. Zhang and H. J. Fan, *Adv. Energy Mater.*, 2013, **3**, 737.

19 T. Yoon, C. Chae, Y.-K. Sun, X. Zhao, H. H. Kung and J. K. Lee, *J. Mater. Chem.*, 2011, **21**, 17325.

20 X. Fang, C. Hua, X. Guo, Y. Hu, Z. Wang, X. Gao, F. Wu, J. Wang and L. Chen, *Electrochim. Acta*, 2012, **81**, 155.